Magnetic-field-induced quadrupolar ordering and the crystal electric field effect in the distorted kagome lattice antiferromagnet $Dy_3Ru_4Al_{12}$

Isao Ishii,* Takuyou Mizuno, Kohki Takezawa, Soichiro Kumano, Yo Kawamoto, and Takashi Suzuki†
Department of Quantum Matter, ADSM, Hiroshima University, Higashi-Hiroshima 739-8530, Japan

Denis I. Gorbunov
Hochfeld-Magnetlabor Dresden (HLD-EMFL), Helmholtz-Zentrum Dresden-Rossendorf, 01328 Dresden, Germany

Margarida S. Henriques and Alexander V. Andreev
Institute of Physics, Academy of Sciences, Na Slovance 2, 182 21 Prague, Czech Republic

(Received 30 March 2018; published 18 June 2018)

To investigate the $4f$-electronic states under a crystal electric field (CEF) and the phase transition in $Dy_3Ru_4Al_{12}$ with the antiferromagnetic transition temperature $T_N = 7$ K, we performed ultrasonic measurements on a single-crystalline sample at zero magnetic field and under fields. The transverse elastic modulus C_{44} shows a characteristic elastic softening. The CEF analyses indicate that the softening is caused by an interlevel quadrupole interaction between the ground and excited Kramers doublets. Under fields, we found a magnetic-field-induced phase transition along both the [100] and [001] directions in addition to the antiferromagnetic ordering. A plausible origin of the field-induced transition is quadrupolar ordering, which is estimated from our CEF calculation. These results and the negative sign of a quadrupole-quadrupole coupling constant suggest that the effect of geometrical frustration alignment due to the kagome lattice also appears on the electric quadrupoles of the Dy ions with the antiferroquadrupolar-type interaction.

DOI: 10.1103/PhysRevB.97.235130

I. INTRODUCTION

Geometrical frustration of spins is one of the themes, which is studied with much attention for fascinating magnetic properties. Antiferromagnetically interacted spins on a triangular lattice, such as a kagome lattice, are its typical candidates for investigating this theme [1–5]. In the rare-earth compounds $R_3Ru_4Al_{12}$ (R: rare earth), which have the hexagonal $Gd_3Ru_4Al_{12}$-type structure (space group $P6_3/mmc$) at room temperature, the R atoms form a distorted kagome net [6–13]. The R-Al and Ru-Al layers are stacked perpendicular to the [001] axis alternately. $R_3Ru_4Al_{12}$ have attracted attention from the viewpoint of the effect of geometrical frustration.

Among them, we paid attention to the Dy-based $Dy_3Ru_4Al_{12}$, of which the phase transition at $T_N = 7$ K was reported by the specific heat measurement [9]. Since hysteresis was detected in the temperature T sweep by thermal expansion measurements, the transition is of the first order [10]. There is no structural transformation at T_N in low temperature x-ray diffraction measurements. As for the origin of the phase transition at T_N, the magnetic susceptibility along the magnetically easy [001] axis shows a cusp-type anomaly at T_N. By neutron diffraction experiments, the magnetic reflection was obtained below T_N. The phase transition at T_N was proposed as an antiferromagnetic (AFM) ordering with a noncollinear magnetic structure [9]. In magnetization curves, one and two metamagnetic phase transitions accompanied by hysteresis were observed in the magnetic field H, along the [100] and [001] axes, respectively. The hysteresis at 2 K becomes small with increasing T.

Meanwhile, many compounds with localized f electrons show exotic physical properties originating from orbital (electric quadrupole) degrees of freedom, such as multipolar ordering [14,15]. The effect of a quadrupole interaction sometimes appears in $4f$-electronic states under a crystal electric field (CEF), because degenerate states of the CEF may have orbital degrees of freedom. The Curie-Weiss law can be applied to the magnetic susceptibility above 100 K along the [100] axis and above 170 K along the [001] axis in $Dy_3Ru_4Al_{12}$ [9]. This means that $4f$ electrons are almost localized. The effective magnetic moments were estimated to be 10.1 μ_B for both axes. These values are approximately the same with the value of the free Dy^{3+} ion (10.6 μ_B). $Dy_3Ru_4Al_{12}$ has the CEF effect with localized f electrons. The sixteenfold multiplet of the Dy^{3+} ion (the total angular momentum $J = 15/2$) splits into eight Kramers doublets under the hexagonal CEF.

In our previous work, we performed ultrasonic measurements of the elastic moduli C_{11} and C_{44} on $Dy_3Ru_4Al_{12}$ and reported a characteristic elastic softening of C_{44} owing to the CEF effect [16]. Although it is common sense that all Kramers doublets have no quadrupole degeneracy, the elastic softening of $Dy_3Ru_4Al_{12}$ may occur due to an interlevel quadrupole interaction between the ground and excited doublets. The ultrasonic technique is a powerful tool to investigate the quadrupole

*ish@hiroshima-u.ac.jp
†Also at Institute for Advanced Materials Research, and Cryogenics and Instrumental Analysis Division, N-BARD, Hiroshima University, Higashi-Hiroshima 739-8530, Japan; tsuzuki@hiroshima-u.ac.jp

interaction, because a strain induced by ultrasound bilinearly couples to a corresponding quadrupole moment [17–19]. In the hexagonal symmetry, C_{44} is the linear responses to the ε_{yz} and ε_{zx} strains which couple to the electric quadrupoles O_{yz} and O_{zx}, respectively. The characteristic softening of C_{44} may be due to the interlevel quadrupole interaction under the hexagonal CEF, suggesting that the magnitude of the interaction of O_{yz} and/or O_{zx} is rather large. Since the softening continues down to T_N, it is expected that the first excited doublet exists at the low energy region, however, the CEF energy states are unclear at present.

Under H, if the interlevel quadrupole interaction enhances by approaching the ground and excited states with increasing H and/or by mixing wave functions of the ground doublet, there is a possibility that magnetic-field-induced quadrupolar ordering emerges, such as $PrOs_4Sb_{12}$ and $HoFe_2Al_{10}$ [20,21]. In the present work, to investigate the $4f$-electronic states under the hexagonal CEF and whether a magnetic-field-induced phase transition occurs, we carried out ultrasonic measurements on $Dy_3Ru_4Al_{12}$ at zero magnetic field and under fields.

II. EXPERIMENTAL DETAILS

Single-crystalline $Dy_3Ru_4Al_{12}$ was grown by a modified Czochralski method. Details of the sample preparation were already reported [9]. The T dependences of the elastic moduli C_{11}, C_{33}, C_{44}, and C_{66} were measured from 0.5 to 150 K. The moduli C_{11} and C_{33} are the longitudinal modes propagating along the [100] and [001] axes, respectively. The transverse moduli C_{44} and C_{66} are the modes propagating along the [100] axis with the polarization direction along the [001] axis and in the [001] plane, respectively. The absolute value of C was estimated at 4.2 K using $C = \rho v^2$, where $\rho = 6.427$ g/cm^3 is the mass density at room temperature and v is the sound velocity in a sample. The change of v was detected by using the phase comparison-type pulse echo method [22]. We also measured T and H dependences of elastic moduli up to 14 T in H along the [100] and [001] axes using a superconducting magnet.

III. RESULTS AND DISCUSSION

A. Elastic moduli at zero magnetic field

The T dependences of the longitudinal elastic moduli C_{11} and C_{33} in $Dy_3Ru_4Al_{12}$ are shown in Fig. 1. With decreasing T, a monotonic hardening of the longitudinal moduli is observed down to T_N without a clear anomaly. There is no elastic softening at high temperatures. At T_N, both moduli exhibit an abrupt elastic hardening, as shown in the insets of Fig. 1.

Figure 2 shows the T dependences of the transverse elastic moduli C_{44} and C_{66} in $Dy_3Ru_4Al_{12}$. The modulus C_{44} displays a large elastic softening below 100 K with decreasing T. The softening continues down to T_N with about 12% reduction of the stiffness, and then C_{44} hardens at T_N. Another elastic softening is observed below 6 K, and it stops around 2 K, as shown in the inset of Fig. 2. (Notice: From repeated ultrasonic measurements on $Dy_3Ru_4Al_{12}$, we correct the temperature at which the softening begins in C_{44} from the data previously reported [16].) In contrast, C_{66} increases monotonically with

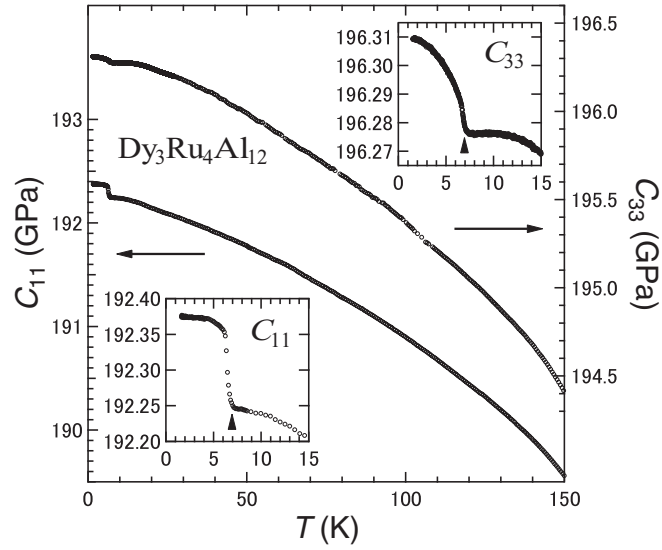

FIG. 1. T dependences of the longitudinal elastic moduli C_{11} and C_{33} in $Dy_3Ru_4Al_{12}$. The insets show the vicinity of T_N below 15 K. The arrow in the insets indicates the phase transition at T_N. C_{11} is the same with the data previously reported [16].

decreasing T at high temperatures. With further decreasing T, C_{66} exhibits an abrupt elastic hardening at T_N.

At the antiferromagnetic transition temperature T_N, all moduli show the abrupt elastic hardening. The hardening indicates a strong coupling between a strain and a magnetic order parameter. This is consistent with the results of the thermal expansion which show steplike lattice contraction at T_N by a magnetoelastic coupling [10]. By considering the thermodynamic theory of elastic modulus with the Landau theory, the abrupt hardening can be understood by a coupling linear in the magnetic order parameter Q but quadratic in the strain ε^2, $g_s Q\varepsilon^2$, where g_s is a coupling constant [23].

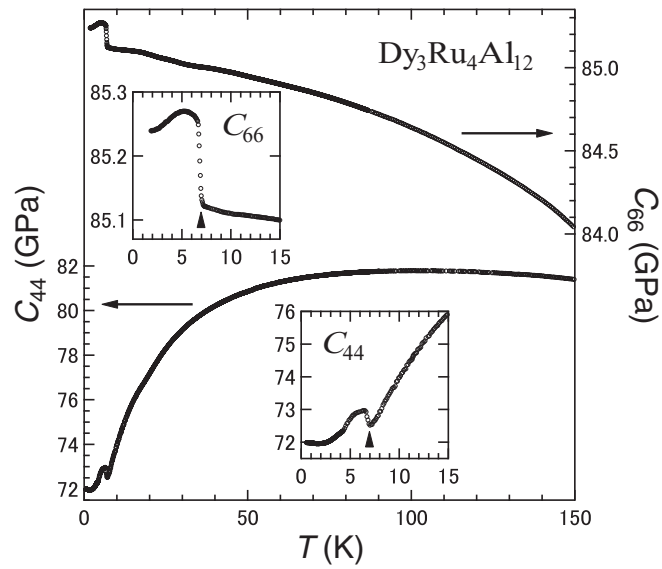

FIG. 2. T dependences of the transverse elastic moduli C_{44} and C_{66} in $Dy_3Ru_4Al_{12}$. The insets show the vicinity of T_N below 15 K. The arrow in the insets indicates the phase transition at T_N.

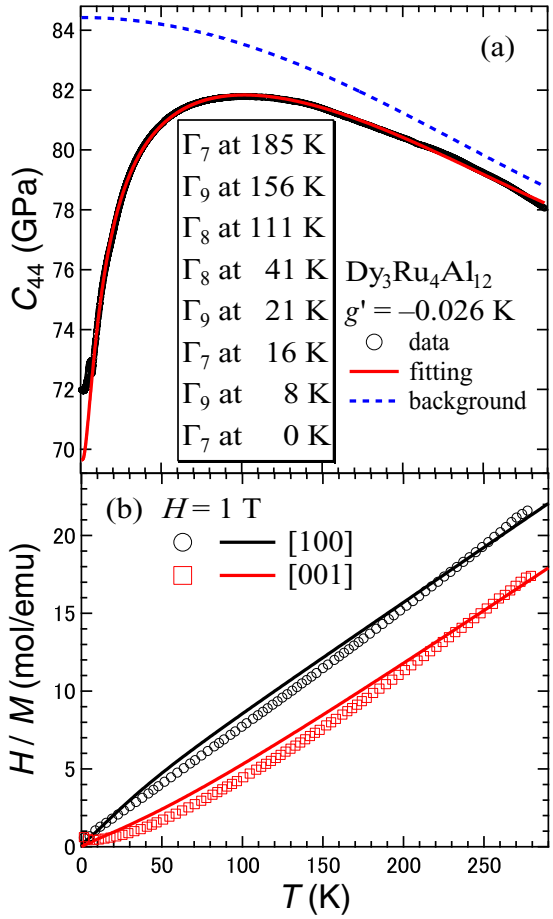

FIG. 3. (a) T dependence of the transverse elastic modulus C_{44} in $Dy_3Ru_4Al_{12}$. The red solid and blue broken curves represent the fitting result and background stiffness, respectively. The inset demonstrates the CEF level scheme from the ground state doublet Γ_7 to the seventh excited state doublet Γ_7 with a corresponding excitation energy obtained by using the CEF parameters listed in Table I. (b) T dependences of the inverse magnetic susceptibility along the [100] and [001] axes. The solid curves demonstrate the best fit. The data are the same as the data previously reported [9].

B. Crystal electric field effect

The softening between T_N and 100 K in C_{44} is a characteristic behavior originating from a quadrupole interaction under the CEF. To confirm elastic behaviors above 150 K, we measured C_{44} between 150 and 290 K. A monotonic hardening with decreasing T is observed above 150 K, as shown in Fig. 3(a). We performed a theoretical fitting of the elastic modulus C_{44} and the inverse magnetic susceptibility above T_N, i.e., in the nonordered state. We considered the effective Hamiltonian $H_{\rm eff}$ for the elastic modulus:

$$H_{\rm eff} = H_{\rm CEF} - \sum_i g_i O_i \varepsilon_i - \sum_i g_i' \langle O_i \rangle O_i \qquad (1)$$

$$H_{\rm CEF} = B_2^0 O_2^0 + B_4^0 O_4^0 + B_6^0 O_6^0 + B_6^6 O_6^6, \qquad (2)$$

where ε_i, g_i, and g_i' are a strain, a strain-quadrupole coupling constant, and a quadrupole-quadrupole coupling constant, respectively. Here, the subscript i is equal to yz or zx, because C_{44} is the linear responses to the ε_{yz} and ε_{zx} strains, which couple to the electric quadrupoles O_{yz} and O_{zx}, respectively. The T dependence of the elastic modulus, $C_{ii}(T)$, is expressed by the following equation:

$$C_{ii}(T) = \frac{-N_0 g_i^2 \chi_s(T)}{1 - g_i' \chi_s(T)} + C_0(T), \qquad (3)$$

where N_0 (=9.548 × 10^{27} m^{-3}) is the number density of Dy ions per unit volume at room temperature and χ_s is the so-called strain susceptibility [24]. Generally, the elastic modulus increases monotonically with decreasing T in compounds without the CEF effect or other instabilities of the structure or the electronic state. We presumed the background stiffness to be

$$C_0(T) = a + bT^2 + cT^4, \qquad (4)$$

where a, b, and c are coefficients determined by the fitting. This equation consists of the phonon contribution $\propto T^4$ and normal electrons $\propto T^2$ terms [25].

The red solid curve in Fig. 3(a) is the best fit. The softening of C_{44} above T_N is well reproduced by the strain susceptibility with fitting parameters listed in Tables I and II. These parameters were determined to reproduce not only the elastic softening of C_{44} at zero magnetic field but also that under fields qualitatively, as explained in detail in Secs. III C and III D. Under the hexagonal CEF, the $4f$-electronic state of the Dy^{3+} ion ($J = 15/2$) splits into eight Kramers doublets which have no quadrupole degeneracy. Since no elastic softening occurs by only the ground doublet, this fitting result reveals that the softening originates from the interlevel quadrupole interaction between the ground and excited doublets. In addition, the magnitude of the quadrupole interaction of O_{yz} and/or O_{zx} is rather large, because C_{44} exhibits the large softening. The negative sign of g_i' indicates an antiferroquadrupolar-type interaction between them.

The inverse magnetic susceptibility above T_N was calculated using the CEF model in the usual manner [26]. Figure 3(b) shows fitting results of the inverse magnetic susceptibility. The data along the [100] and [001] axes are qualitatively reproduced. We obtained the CEF level scheme: the ground doublet Γ_7, the first excited doublet Γ_9 at 8 K, the second excited doublet Γ_7 at 16 K, and the third excited doublet Γ_9 at 21 K, as shown in the inset of Fig. 3(a).

TABLE I. CEF parameters of $Dy_3Ru_4Al_{12}$.

B_2^0 (K)	B_4^0 (K)	B_6^0 (K)	B_6^6 (K)
−0.89	3.80×10^{-3}	-1.60×10^{-5}	2.00×10^{-4}

TABLE II. Fitting parameters of C_{44}: $|g_i|$ (K), g_i' (K), a (GPa), b ($\times 10^{-5}$ GPa/K^2), and c ($\times 10^{-10}$ GPa/K^4).

	$\lvert g_i \rvert$	g_i'	a	b	c
C_{44}	64.6	-2.60×10^{-2}	84.4	−9.05	2.71

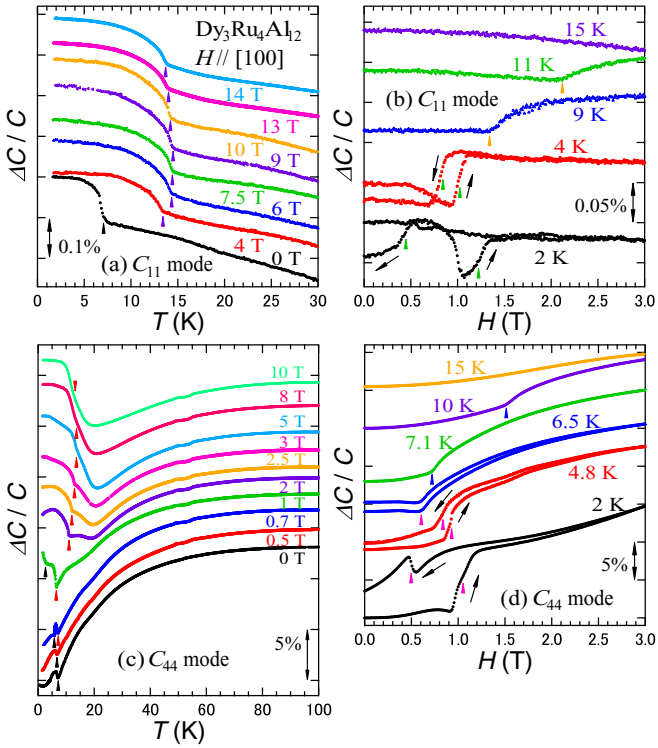

FIG. 4. T and H dependences of the elastic moduli (a),(b) C_{11} and (c),(d) C_{44} along $H||[100]$ at various conditions in $Dy_3Ru_4Al_{12}$. We plotted the data adding a constant value to easily see each data curve. The arrows indicate the phase transitions.

C. Magnetic field-temperature phase diagram

To investigate the ordered state in $Dy_3Ru_4Al_{12}$, we performed ultrasonic measurements under magnetic fields. Figures 4(a) and 4(b) show the T and H dependences of the elastic modulus C_{11}, respectively, along $H||[100]$. The T dependence of C_{11} at zero field displays the abrupt hardening at T_N. Above 4 T, an elastic hardening accompanied by a clear inflection point is detected in the vicinity of 14 K, which is a quite higher temperature than T_N. We defined the temperature of the inflection point as another phase transition temperature, T_Q, along $H||[100]$ and the highest T_Q is 14.4 K at 9 T. In the H dependences of C_{11} at 2 and 4 K below T_N shown in Fig. 4(b), obvious hysteresis owing to the antiferromagnetic ordering is observed below 1.5 T as is the case with the magnetization curves [9]. In contrast, above T_N, C_{11} at 9 K exhibits an inflection point at 1.3 T. The magnetic field of the inflection point increases with increasing T, and no elastic anomaly is seen at 15 K. The inflection point at T_Q is not accompanied by hysteresis, suggesting that the phase transition at T_Q is of the second order.

We measured the T and H dependences of C_{44} in order to clarify T_Q in detail. At zero field, the elastic softening below 100 K stops at T_N in the T dependence of C_{44}, as shown in Fig. 4(c). T_N decreases with increasing H at low fields, and there are two anomalies at 0.7 and 1 T. Above 2 T, C_{44} exhibits an inflection point at T_Q up to 10 T accompanied by a broad minimum around 20 K. The magnitude of the softening decreases gradually with increasing H. The H dependences of C_{44} at various temperatures are shown in Fig. 4(d). The

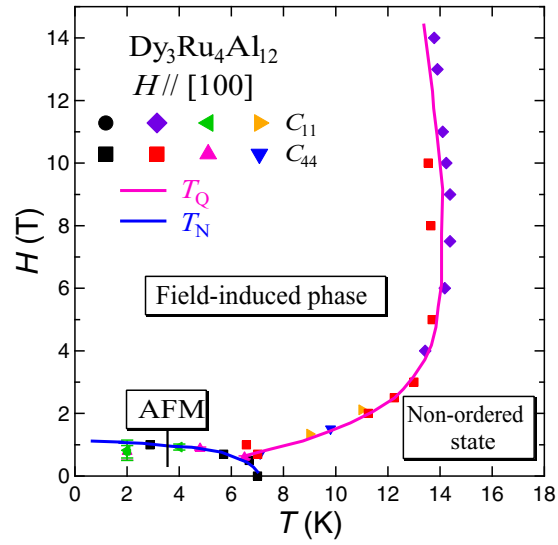

FIG. 5. The H-T phase diagram along $H||[100]$ in $Dy_3Ru_4Al_{12}$. The solid curves are guides for the eyes. The middle point of hysteresis is defined as T_N, and the hysteresis is depicted by an error bar.

modulus C_{44} below T_N displays large hysteresis as well as C_{11}. Above T_N, an inflection point of C_{44} is also detected. The magnetic field of the inflection point at T_Q increases with increasing T, and T_Q is not observed at 15 K.

From the T and H dependences of the elastic moduli we drew the H-T phase diagram of $Dy_3Ru_4Al_{12}$ for the [100] axis, as shown in Fig. 5. T_N decreases monotonically with increasing H and the antiferromagnetic phase boundary closes around 1 T. On the other hand, a magnetic-field-induced phase transition at T_Q appears above 1 T. T_Q increases with increasing H, and the highest T_Q is 14.4 K at 9 T. With further increasing H, T_Q decreases gradually and the phase boundary does not close up to 14 T. The origin of the field-induced phase transition will be discussed in Sec. III D.

The T and H dependences of the elastic modulus C_{33} along $H||[001]$ are shown in Figs. 6(a) and 6(b), respectively. At zero field, there is an abrupt elastic hardening at T_N in the T dependence of C_{33}. The abrupt hardening becomes large at 0.5 and 0.9 T. Above 5 T, no hardening at T_N appears, however, C_{33} displays a slight elastic softening below 6 K and a minimum in the vicinity of 4 K. We defined the temperature of the minimum as T_Q along $H||[001]$. T_Q decreases with increasing H up to 14 T. In the H dependences of C_{33} below T_N, two clear hysteresis originating from the phase transitions within magnetically ordered states are observed below 1.5 T, as shown in Fig. 6(b). The magnetic fields of the hysteresis decrease with increasing T. These results are consistent with the data in the magnetization [9]. No elastic anomaly is detected at 10 K in C_{33} along $H||[001]$ in contrast to the elastic moduli along $H||[100]$.

Figure 6(c) shows the T dependences of C_{44} along $H||[001]$. Above 1.5 T, although the H dependences of C_{33} exhibit no elastic anomaly due to the magnetic transitions, a sharp downward peak indicating another phase transition is detected below 5 K. The temperature of the peak, which corresponds to the minimum of C_{33} (T_Q), decreases with increasing H. As shown in Fig. 6(d), two elastic anomalies

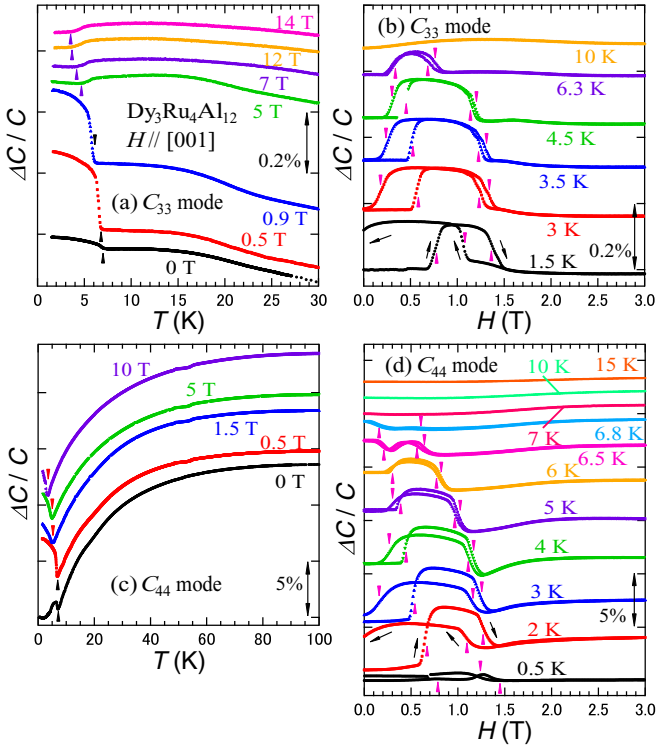

FIG. 6. T and H dependences of the elastic moduli (a),(b) C_{33} and (c),(d) C_{44} along $H||[001]$ at various conditions in $Dy_3Ru_4Al_{12}$. The curves are vertically offset for clarity. The arrows indicate the phase transitions.

accompanied by hysteresis emerge in the H dependences of C_{44} below T_N as well as C_{33}. There is no anomaly above T_N.

From these results, the H-T phase diagram of $Dy_3Ru_4Al_{12}$ for the [001] axis and its closeup below 1.6 T are shown in Figs. 7(a) and 7(b), respectively. The antiferromagnetic phase boundary and its metamagnetic ordered one close around 0.4 and 1.3 T, respectively. Meanwhile, there is a magnetic-field-induced phase transition at T_Q above 1.5 T along $H||[001]$. T_Q decreases gradually with increasing H and survives up to

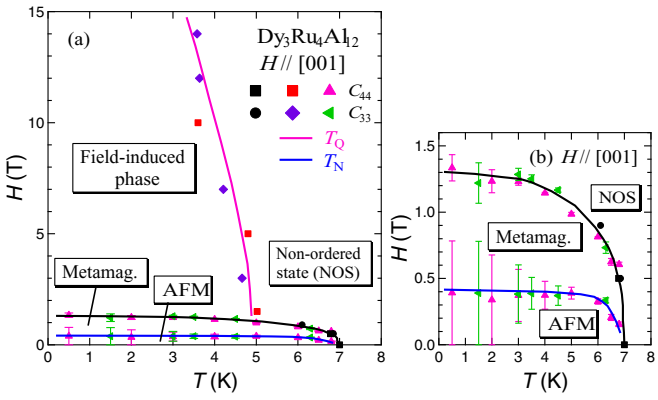

FIG. 7. (a) The H-T phase diagram along $H||[001]$ in $Dy_3Ru_4Al_{12}$. The solid curves are guides for the eyes. (b) The same phase diagram in an expanded scale below 1.6 T. The middle point of the hysteresis is defined as the magnetic phase transitions, and the hysteresis is represented by an error bar.

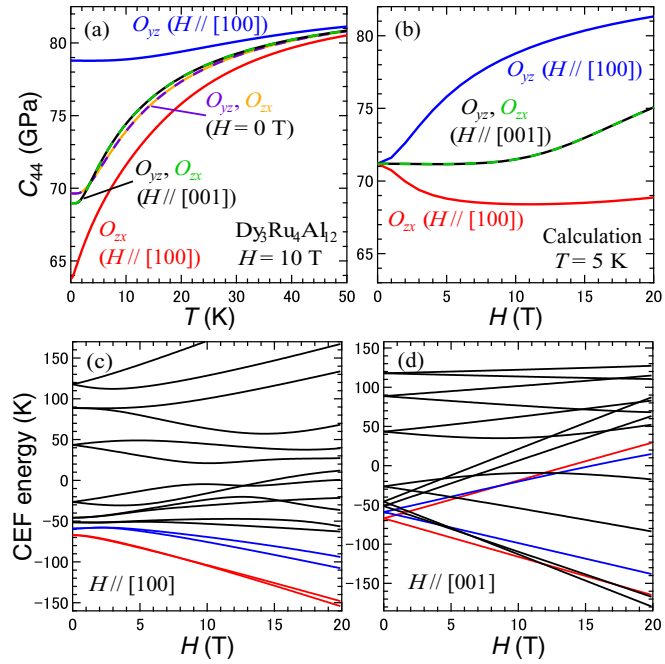

FIG. 8. (a) T and (b) H dependences of the calculated C_{44} along $H||[100]$ and $H||[001]$, for instance, at 10 T and at 5 K, respectively. The H dependences of the calculated CEF energies along (c) $H||[100]$ and (d) $H||[001]$. The ground and the first excited doublets are depicted by the red and blue solid curves, respectively.

14 T. Consequently, we clarified the H-T phase diagram along the [100] and [001] axes and found the magnetic-field-induced phase transition at T_Q in both magnetic field directions.

D. Magnetic-field-induced phase transition

Hereafter, we discuss the origin of the magnetic-field-induced phase transition along both $H||[100]$ and $H||[001]$ from the viewpoint of a magnetic-field-induced quadrupolar ordering. In our measurements, the modulus C_{44} as a function of temperature shows a large elastic softening with 12% reduction of the stiffness arising from the interlevel quadrupole interaction between the ground and excited doublets. The softening is also observed under magnetic fields. The modulus C_{44} is the linear responses to the ε_{yz} and ε_{zx} strains which couple to quadrupoles O_{yz} and O_{zx}, respectively, because C_{44} and C_{55} are degenerate in the hexagonal symmetry. If the expected value of the quadrupole interaction between the ground and exited states emerges and/or becomes large with increasing H, magnetic-field-induced quadrupolar ordering may occur.

We calculated C_{44} under $H||[100]$ and $H||[001]$ in the nonordered state for both quadrupoles O_{yz} and O_{zx} using Eq. (1) and the Zeeman term. Figures 8(a) and 8(b) show the T and H dependences of the calculated C_{44}, respectively, under fields. At zero field, the calculated values for both O_{yz} and O_{zx} are the same and show a constant value below 2 K because of no quadrupole interaction within the ground doublet.

Along $H||[100]$, however, the softening is enhanced in the calculated C_{44} for O_{zx} in contrast to that for O_{yz} with a reduction of the softening with increasing H, as shown in

Fig. 8(a). The H dependence of the calculated C_{44} for O_{zx} displays the softening with increasing H, indicating enhancement of the quadrupole interaction. There is a monotonic hardening in the calculated C_{44} for O_{yz}. These behaviors can be explained by the H dependences of the CEF energies, which are calculated by using Eq. (2) and the Zeeman term, as shown in Fig. 8(c). The energy splitting of the ground doublet is very small by applying $H||[100]$. Since wave functions of the $4f$-electronic states are mixed by the Zeeman interaction, the ground doublet possesses the quadrupole interaction of O_{zx} under $H||[100]$. The quadrupole interaction of O_{zx} enhances with increasing $H||[100]$ below 10 T. Above 10 T, the ground doublet splits gradually, suggesting that the magnitude of the quadrupole interaction starts to decrease. The temperature of the field-induced phase transition increases below 10 T and decreases gradually above 10 T, as shown in Fig. 5.

In contrast, no quadrupole interaction of O_{yz} exists within the ground doublet. The energy splitting between the ground and the first excited doublets becomes large with increasing $H||[100]$, indicating a reduction of the interaction of O_{yz}. Therefore, the magnitude of the softening in the calculated C_{44} for O_{yz} decreases with increasing H. From these results, we propose that the magnetic-field-induced phase transition along $H||[100]$ is the quadrupolar ordering of O_{zx}. In the data of C_{44} shown in Fig. 4(c), the softening stops above the field-induced phase transition temperature. This may be caused by the experimental setting, meaning that the present setting does not detect a response of the quadrupole O_{zx} along $H||[100]$, because the magnetic field along $H||[100]$ breaks the crystal symmetry in the [001] plane and the degeneracy between O_{yz} and O_{zx}.

On the other hand, along $H||[001]$, O_{yz} and O_{zx} are degenerate and the calculated results for both O_{yz} and O_{zx} exhibit the same behaviors, as shown in Figs. 8(a) and 8(b). The softening continues down to 2 K, and the magnitude of the softening below 10 T is nearly the same with that at zero field in the calculated T dependences. The H dependences of the calculated C_{44} display an elastic hardening above 10 T gradually. These behaviors can also be understood by the H dependences of the CEF energies. As shown in Fig. 8(d), one state of the excited doublet approaches the ground state with increasing $H||[001]$, and the interlevel quadrupole interaction exists between them. No quadrupole interaction of O_{yz} and O_{zx} emerges within the ground doublet under $H||[001]$. In both experimental results and calculation, the magnitude of the softening (i.e., the quadrupole interaction) under fields is nearly the same as the softening magnitude at zero field. The softening of the calculated C_{44} continues down to 2 K. The field-induced phase transition along $H||[001]$ appears above the magnetic field at which the magnetic transitions vanish, as shown in Fig. 7. Although the origin of magnetic-field-induced phase transition is unclear at present, there is a possibility that the field-induced phase transition along $H||[001]$ is the quadrupolar ordering of O_{yz} or O_{zx} by approaching the ground and excited states.

The antiferroquadrupolar-type coupling constant between the quadrupole moments ($g_i' < 0$) is obtained by our CEF analyses. In the case of antiferroquadrupolar ordering, a geometrically frustrated alignment of the electric quadrupole is expected, because the electric quadrupole stays on each Dy ion of the kagome lattice. To clarify whether the ordered structure under fields is quadrupolar ordering and whether there is an influence of the geometrical frustration on the quadrupolar system, neutron diffraction and/or resonant x-ray scattering experiments under fields and theoretical studies are needed.

IV. CONCLUSION

We measured the elastic moduli of the distorted kagome lattice antiferromagnet $Dy_3Ru_4Al_{12}$. The large elastic softening arising from the interlevel quadrupole interaction was detected in the transverse modulus C_{44} at zero field. We analyzed the hexagonal CEF effect in $Dy_3Ru_4Al_{12}$, and then the obtained CEF level scheme is the ground doublet Γ_7, the first excited doublet Γ_9 at 8 K, and so on. Ultrasonic measurements under fields reveal that the magnetic-field-induced phase transition exists at high fields along both $H||[100]$ and $H||[001]$. These phase boundaries do not close up to 14 T. From calculation by using the obtained CEF parameters, we propose that the magnetic-field-induced phase transition is caused by the quadrupole interaction and the order parameter along $H||[100]$ may be the quadrupole O_{zx}.

ACKNOWLEDGMENTS

This work was supported by JSPS KAKENHI Grants No. 17H06136. This work was also supported by CResCent (Chirality Research Center) in Hiroshima University (the MEXT program for promoting the enhancement of research universities, Japan). We acknowledge the support of the Czech Science Foundation (Projects No. 14-03276S and No. 16-03593S), Materials Growth and Measurement Laboratory (MGML, https://mgml.eu), and High Magnetic Field Laboratory (HLD) at Helmholtz-Zentrum Dresden-Rossendorf (HZDR), a member of the European Magnetic Field Laboratory (EMFL). A part of this work was also funded by the National Sustainability Programme I of Czech Republic (Project No. LO1603) under the Ministry of Education, Youth, and Sports.

[1] A. P. Ramirez, Annu. Rev. Mater. Sci. **24**, 453 (1994).
[2] R. Moessner and J. T. Chalker, Phys. Rev. B **58**, 12049 (1998).
[3] R. Moessner and A. P. Ramirez, Phys. Today **59**, 24 (2006).
[4] Y. Okamoto, H. Yoshida, and Z. Hiroi, J. Phys. Soc. Jpn. **78**, 033701 (2009).
[5] K. Sengupta, M. K. Forthaus, H. Kubo, K. Katoh, K. Umeo, T. Takabatake, and M. M. Abd-Elmeguid, Phys. Rev. B **81**, 125129 (2010).
[6] J. Niermann and W. Jeitschko, Z. Anorg. Allg. Chem. **628**, 2549 (2002).
[7] W. Ge, H. Ohta, C. Michioka, and K. Yoshimura, J. Phys.: Conf. Ser. **344**, 012023 (2012).

[8] D. I. Gorbunov, M. S. Henriques, A. V. Andreev, V. Eigner, A. Gukasov, X. Fabrèges, Y. Skourski, V. Petříček, and J. Wosnitza, Phys. Rev. B **93**, 024407 (2016).
[9] D. I. Gorbunov, M. S. Henriques, A. V. Andreev, A. Gukasov, V. Petříček, N. V. Baranov, Y. Skourski, V. Eigner, M. Paukov, J. Prokleška, and A. P. Gonçalves, Phys. Rev. B **90**, 094405 (2014).
[10] M. S. Henriques, D. I. Gorbunov, D. Kriegner, M. Vališka, A. V. Andreev, and Z. Matěj, J. Magn. Magn. Mater. **400**, 125 (2016).
[11] V. Chandragiri, K. K. Iyer, and E. V. Sampathkumaran, Intermetallics **76**, 26 (2016).
[12] D. I. Gorbunov, M. S. Henriques, A. V. Andreev, Y. Skourski, and M. Dušek, J. Alloys Compd. **634**, 115 (2015).
[13] S. Nakamura, S. Toyoshima, N. Kabeya, K. Katoh, T. Nojima, and A. Ochiai, Phys. Rev. B **91**, 214426 (2015).
[14] H. Sato, H. Sugawara, Y. Aoki, and H. Harima, in *Handbook of Magnetic Materials*, edited by K. H. J. Buschow (North Holland, Amsterdam, 2009), Vol. 18, Chap. 1.
[15] T. Onimaru and H. Kusunose, J. Phys. Soc. Jpn. **85**, 082002 (2016).
[16] I. Ishii, K. Takezawa, H. Goto, S. Kamikawa, A. V. Andreev, D. I. Gorbunov, M. S. Henriques, and T. Suzuki, J. Phys.: Conf. Ser. **807**, 012002 (2017).
[17] I. Ishii, H. Muneshige, Y. Suetomi, T. K. Fujita, T. Onimaru, K. T. Matsumoto, T. Takabatake, K. Araki, M. Akatsu, Y. Nemoto, T. Goto, and T. Suzuki, J. Phys. Soc. Jpn. **80**, 093601 (2011).
[18] I. Ishii, H. Muneshige, S. Kamikawa, T. K. Fujita, T. Onimaru, N. Nagasawa, T. Takabatake, T. Suzuki, G. Ano, M. Akatsu, Y. Nemoto, and T. Goto, Phys. Rev. B **87**, 205106 (2013).
[19] I. Ishii, K. Takezawa, T. Mizuno, S. Kamikawa, H. Ninomiya, Y. Matsumoto, S. Ohara, K. Mitsumoto, and T. Suzuki, J. Phys. Soc. Jpn. **87**, 013602 (2018).
[20] M. Kohgi, K. Iwasa, M. Nakajima, N. Metoki, S. Araki, N. Bernhoeft, J. M. Mignot, A. Gukasov, H. Sato, Y. Aoki, and H. Sugawara, J. Phys. Soc. Jpn. **72**, 1002 (2003).
[21] S. Kamikawa, I. Ishii, K. Takezawa, T. Sakami, F. Nakagawa, H. Tanida, M. Sera, and T. Suzuki, J. Phys. Soc. Jpn. **86**, 044601 (2017).
[22] T. J. Moran and B. Lüthi, Phys. Rev. **187**, 710 (1969).
[23] W. Rehwald, Adv. Phys. **22**, 721 (1973).
[24] B. Lüthi, in *Dynamical Properties of Solids*, edited by G. K. Horton and A. A. Maradudin (North-Holland, Amsterdam, 1980), Chap. 4.
[25] M. Nohara, T. Suzuki, Y. Maeno, T. Fujita, I. Tanaka, and H. Kojima, Phys. Rev. B **52**, 570 (1995).
[26] S. Kamikawa, I. Ishii, Y. Noguchi, H. Goto, T. K. Fujita, F. Nakagawa, H. Tanida, M. Sera, and T. Suzuki, J. Phys. Soc. Jpn. **85**, 074604 (2016).